JOINT ANALYTICAL - MONTE CARLO TRANSPORT ANALYSIS OF THE IRR1 NEUTRON CAMERA ENABLING RAPID REACTOR OPTIMIZATION

U. STEINITZ, A. KRAKOVICH, I. NEDER

Soreq Nuclear Research Centre,
Yavneh, Israel

Abstract

Neutron radiography is a frequent activity of the Israeli Research Reactor 1 (IRR1). As such, a simulation that can predict the neutron imaging flux is a valuable tool. Monte-Carlo codes can accurately compute the flux at the core vicinity, but when the domain contains the whole neutron camera channels, simulations are limited since only a fraction of the simulated neutrons arrive at the imaging plane, and thus the statistical error is large. We report the development of an analytic method based on transport theory which predicts the flux at the imaging plane from Monte Carlo calculations of only the reactor core. We locate the origins of the neutrons propagating ballistically towards the imager, and tally the flux at these sites. This method was validated by comparison with MCNP calculations and with past measurements. We show that this method may help optimize the core for radiography increasing efficiency by 50%.

1 Introduction

In the Israeli Research Reactor 1 (IRR1, Soreq Nuclear Research Centre) there is a frequent use of neutron radiography. In the academic community there is an extensive ongoing effort to calculate neutron flux at a reactor core, but a direct computation of the radiographic performance has additional complexities. The main radiographic device in IRR1 is a neutron camera (NC), a device designed to transfer neutron flux from a source (such as a reactor) onto an imaging plane where the spatial flux distribution is determined by a detector (e. g., film). When an object is placed within the neutron beam near the imaging plane, the recorded image represents the neutron transmission map of the examined object- its neutronic shadow.
Basically, the NC consists of a hollow tube that reaches a high flux zone near the core of a reactor, off which a fraction of the neutrons scatter and propagate ballistically to the detector. In the way, there are some obstacles such as the tube's lid and a neutron filter, which attenuate the beam. A circular aperture increases image sharpness by limiting the angular span of the beam.
An accurate prediction of the flux at the imaging plane in order to better plan future core layouts and optimize reactor effectiveness is warranted. However, the geometric limit set by the aperture and the tube structure in the IRR1 is so stringent that out of 10 million neutrons that enter the tube less than one neutron makes it to the film. This makes modelling of the NC by means of Monte-Carlo (MC) simulations highly ineffective. In this paper we report a method that circumvents this problem by using an analytical analysis based on the transport theory to assess the amount of ballistic neutrons arriving at the film, based on the flux determined through MCNP calculation of the reactor core area.

We use a few assumptions on the flux at the core and derive some simplifications to the integral-differential transport equation that help us to locate the effective source of ballistic neutrons, and explain why calculating the flux only at a few specific points of the source is enough to produce an accurate prediction. We validated our predictions using conventional MCNP analysis, as well as by comparison to past experimental results.

The insights gained by this method allow us to design core layouts that could potentially increase NC flux by 50%.

Following this introduction, this paper presents the analytical Transport + MC method, details some of the method's results and how they compare to other calculations and recent measurements, and conclude with some of the future benefits and experiments that could further validate this model.

2 Transport-MC model

When regarding the neutrons arriving through an aperture to an imaging plane, we consider only the particles that fly ballistically from the channel entrance. This is justified by the fact that the flux diminishes substantially as one retreats from the core, thus, the contribution of additional neutrons scattering off the material in the way is negligible. In this section we consider the high-flux zones, and assess the number of neutrons scattered per unit time, and what is their chance to fly unobstructed to the film.
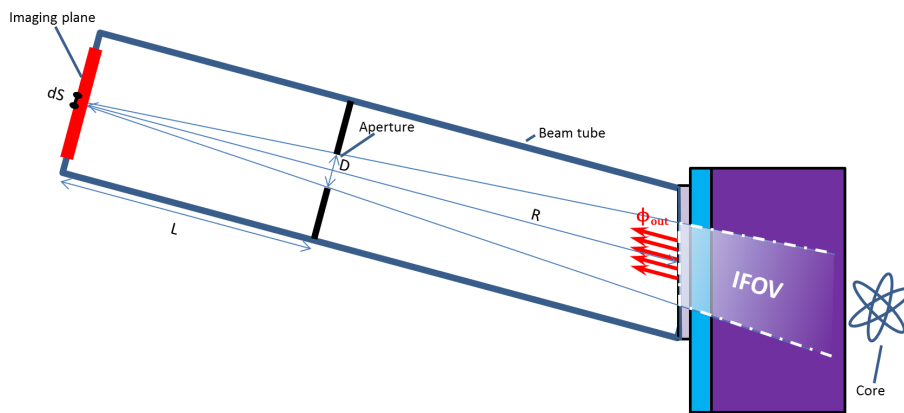
Figure 1: Schematic top view of the neutron camera (not to scale)

The instantaneous-field-of-view (IFOV) is the volume from which neutrons emanate and ballistically propagate to a point on the film ('pixel'). Neutrons come from outside the beam tube, within the cone defined by a vertex at the pixel and a rim that touches the circumference of the circular aperture (see Fig. 1). The particles that emanate from material not within the IFOV cannot reach the film directly as they are absorbed by the aperture material. For a volume element at $\bar{r}$ within the IFOV, The scattering rate density equals the local flux $\Phi(\bar{r})$ multiplied by the local macroscopic scattering cross-section $\Sigma_s(\bar{r})$. From the scattered neutrons we sift only those who scatter to a pixel with area dS (perpendicular to the beam's axis), so if the scattering is isotropic we consider only a fraction of $dS/4\pi |\bar{r} - \bar{r}_{pixel}|^2$. The beam is further diluted by any interaction with the matter (total cross-section Σ_t) leaving only fraction $\exp\left(-|\int \Sigma_t(s)\, ds|\right)$ of the neutrons, where the integral is over the line from the scattering site to the channel's entrance. On top of that, one should add the channel transmission factor A_{ch} (related to the attenuation by materials in the beam path, such as filters, aluminium partitions and air). The

rate of neutrons arriving at the imaging plane for a pixel dS is thus

$$\Phi_{out}dS = A_{ch}\int\limits_{IFOV} dV\,\Phi\left(\bar{r}\right)\Sigma_s\left(\bar{r}\right)\frac{\exp\left(-\left|\int_{\bar{r}}^{\bar{r}_{entrance}}\Sigma_t\left(s\right)ds\right|\right)dS}{4\pi\left|\bar{r}-\bar{r}_{pixel}\right|^2} \quad , \tag{1}$$

which is closely related to the integral transport equation (or Peierls equation [Duderstadt 1979]).

Consider now a practical situation of stacked homogeneous layers with parallel faces perpendicular to the x-axis. We set the origin $x = y = z = 0$ at the point where the IFOV's axis intersects with the interface between the beam tube's lid to the void inside it. The IFOV's axis is slanted by an angle θ (in the $x-y$ plane) to the layers' faces. Application of Eq. (1) for a layer of width W whose closest face is x_0 away from the channel entrance, will lead to the contribution of this layer to the flux at the film, which we denote Φ_{layer}. To leading order in D/L, we find

$$\Phi_{\text{layer}} \approx A_{ch}A\left(x_0\right)\int\limits_{x_0}^{x_0+W}dx\int\limits_{S_s(x)}dydz\,\Phi\left(x,y,z\right)\Sigma_s\frac{\exp\left(-\Sigma_t\left|x-x_0\right|/\cos\theta\right)}{4\pi\left(R+d\right)^2} \quad , \tag{2}$$

where R is the length of the tube (from the pixel on the imaging plane to the origin), $d = x/\cos\theta$ is the length of a path between a point (x,y,z) in the layer to the plane x=0, at angle θ from this plane (see Fig. 2). Note that the distance that a neutron travelling from any point on a plane $x = \text{constant}$ in the IFOV, through the aperture, to the imaging plane, is $\sim R+d$ up to additional terms of order D/L, which we neglect. The area in depth x within the IFOV is the source area

$$S_s\left(x\right) = \frac{1}{\cos\theta}\frac{\pi}{4}\left[\frac{D\left(R+d\right)}{L}\right]^2 \quad , \tag{3}$$

In addition, The neutrons exiting from x_0 towards the channel are attenuated by the factor of $A\left(x_0\right) = \exp\left(-\left|\int_{x_0}^{0}dx\Sigma_t\left(x\right)/\cos\theta\right|\right)$. We use a constant θ in the cosine terms, justified by the small angular variation $D/L \ll 1$ (in many cases $D/L < 1/100$). We combine Eqs. (2) and (3)
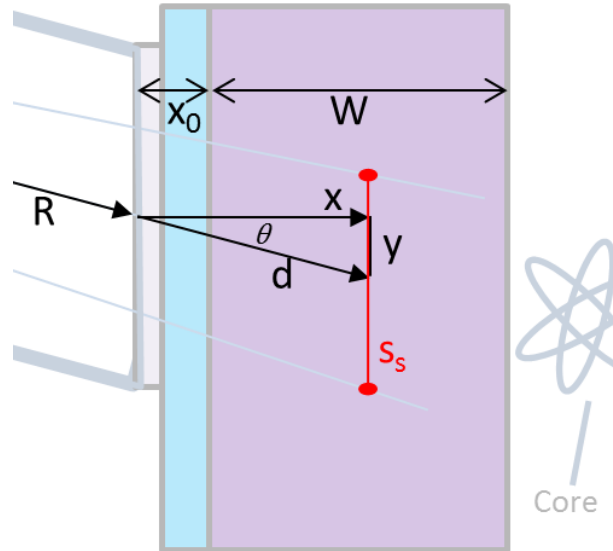
Figure 2: Close-up view of the channel entrance (not to scale)

to get the expression

$$\Phi_{\text{layer}} \approx \frac{A_{ch}A\left(x_0\right)}{\cos\theta}\left(\frac{4L}{D}\right)^{-2}\int\limits_{x_0}^{x_0+W}dx\bar{\Phi}_S\left(x\right)\Sigma_s e^{-\left|\Sigma_t\frac{x-x_0}{\cos\theta}\right|} \quad , \tag{4}$$

in which we introduced the average flux over the source area:

$$\bar{\Phi}_S\left(x\right) = \frac{1}{S_S\left(x\right)} \int\limits_{S_S(x)} dy dz \Phi\left(x, y, z\right) \qquad .$$

So far we have expressed Φ_{layer}, the contribution of a homogeneous layer to the thermal flux arriving at the film in terms of the local flux distribution in the layer. Analysis of the flux distribution (e. g., using MCNP simulations) and summation of the contributions of the different layers will estimate the beam strength at the imaging plane,

$$\Phi_{out} dS = \sum \Phi_{\text{layer}, i} dS.$$

Notice that the exponential attenuation between the layer and the channel entrance $A\left(x_0\right)$ alludes that only few layers have potentially significant contributions, and beyond several mean free paths the ballistic flux is minuscule.

Let us now make some assumptions regarding the flux in a layer. We may choose a linear approximation of the average source flux $\bar{\Phi}_S\left(x\right) = \Phi_0 + \left(x - x_0\right)\Phi'$ where $\Phi_0 = \bar{\Phi}_S\left(x_0\right)$ and $\Phi' = \frac{d}{dx}\bar{\Phi}_S\left(x = x_0\right)$. Our flux calculations (discussed later in this paper) show that this is a reasonable approximation for the layers in question. Substitution in the integral of Eq. (4) produces

$$\Phi_{layer} \approx A_{ch} A\left(x_0\right) \left(\frac{4L}{D}\right)^{-2} \int\limits_0^W dx \left(\Phi_0 + x\Phi'\right) \frac{\Sigma_s}{\cos\theta} e^{-x/\delta} \qquad , \qquad (5)$$

and we have introduced the mean-free-*depth* $\delta = \cos\theta/\Sigma_t$, which have the physical meaning of the average depth (along the x axis) in which a neutron arriving at an angle θ to a layer interacts with the material (the angle varies only slightly for different pixels at the order of the film's side divided by L, so θ is considered constant). The integral in Eq. (5) is solved analytically:

$$\int\limits_0^W dx \left(\Phi_0 + x\Phi'\right) \frac{\Sigma_s}{\cos\theta} e^{-x/\delta} = \frac{\Sigma_s}{\Sigma_t}\left[\left(\Phi_0 + \delta\Phi'\right)\left(1 - e^{-W/\delta}\right) - \Phi' W e^{-W/\delta}\right] \approx$$

$$\approx \frac{\Sigma_s}{\Sigma_t}\left[\left(1 - e^{-W/\delta}\right)\bar{\Phi}_S\left(x_0 + \delta - \frac{W}{e^{W/\delta} - 1}\right)\right] \qquad , \qquad (6)$$

where we used the linear approximation of the average source flux.

The important implication of Eq. (6) is that the contribution of the layer to the total imaging flux is determined using the local flux at a single location, and there is no need for integration. The depth in which the flux should be 'sampled' in each layer is fixed at depth $\delta - \frac{W}{e^{W/\delta} - 1}$ and in the first order approximation depends only on the layer's width and material, and on the channel's angle. There are several cases to consider in this 'layers-model':

- Thin layer ($W/\delta \ll 1$): When the layer is much thinner than the mean free depth, the contribution of the layer is

$$\Phi_{layer} \approx A_{ch} A\left(x_0\right) \left(\frac{4L}{D}\right)^{-2} W \frac{\Sigma_s}{\cos\theta} \bar{\Phi}_S\left(x_0 + \frac{W}{2}\right) \qquad , \qquad (7)$$

where we sample the flux at the centre ($W/2$), which is also the average flux in this layer.

- Thick layer ($W/\delta \gg 1$): For thick layers, the terms containing exponents in Eq (6) vanish, and the sampling site is at the total mean free depth:

$$\Phi_{layer} \approx A_{ch} A\left(x_0\right) \left(\frac{4L}{D}\right)^{-2} \frac{\Sigma_s}{\Sigma_t} \bar{\Phi}_S\left(x_0 + \delta\right) \qquad , \qquad (8)$$

- Medium thickness: In all other cases, we use Eq. (6) directly:

$$\Phi_{layer} \approx A_{ch} A\left(x_0\right) \left(\frac{4L}{D}\right)^{-2} \frac{\Sigma_s}{\Sigma_t} \left(1 - e^{-W/\delta}\right) \bar{\bar{\Phi}}_S \left(x_0 + \delta - \frac{W}{e^{W/\delta} - 1}\right) \qquad . \qquad (9)$$

To summarize, we depict the sampling depth (the deviation from the edge in the argument of $\bar{\bar{\Phi}}_S$ in Eq. (9) for different widths in Fig. 3. We dub this scheme by SALAMI- $\underline{St}\underline{A}$cked $\underline{LA}$yers $\underline{M}$onte-Carlo $\underline{I}$ncident neutron calculation method.
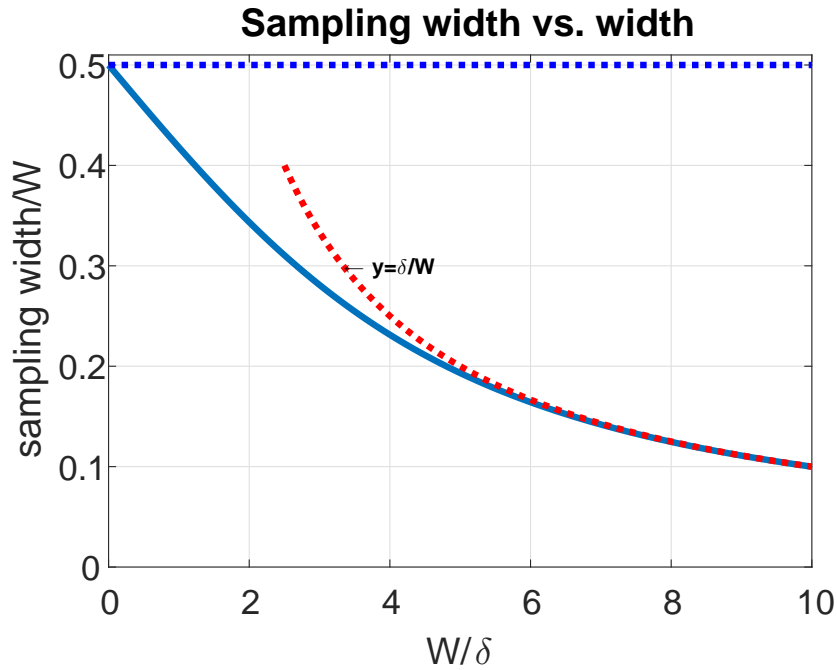
Figure 3: The ratio of sampling depth to layer width (solid) as a function of the width (in units of mean-free-depths δ). dashed curves show the asymptotic behaviour.

3 Results

In an attempt to validate the SALAMI model, we used the full core MCNP simulation of IRR1 [Krakovich 2016], including historic burnup calculation. This simulations allows tallying the flux at different locations, therefore the SALAMI method is easy to implement by choosing the relevant tally sites (see Fig. 4 for a schematic core image). Between the NC channel and the fuel rods there are a few layers, of aluminium, water and graphite. The simulations show that for all the layers the thermal neutron flux is more or less linear with width (see Fig. 5), justifying our use of the Taylor expansion. The beam tube is at angle $\theta = 30^o$, and the water and graphite layers are several mean-free-depths wide, and practically there is no need to consider further layers in the SALAMI-model. The thick graphite layer, even though it has nearly twice the flux than the closest layer, contributes only about 5% of the ballistic neutrons arriving at the film, and we have found that the source of the majority of neutrons is the water layer ($\sim 1\,cm$ thick) in front of the channel.

As discussed in Sec. 1, MCNP simulation of the full channel is not feasible and therefore we compared our predictions with a simulation of the flux at a small, close 'camera'. Its geometry was that of a thin thimble whose axis is collinear with the actual beam tube of the IRR1, its open end facing the core, and its location a few centimetres from it (see small red mark in
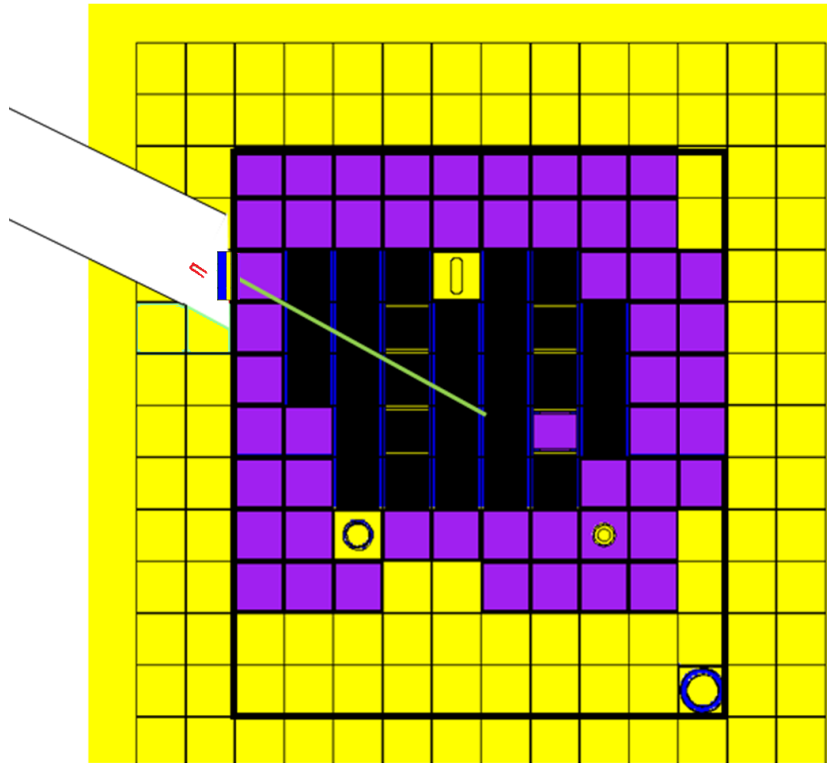
Figure 4: Schematic top view of the IRR1 core at the end of 2015 with the slanted beam tube. Square colour codes: black- fuel; purple- graphite; yellow- water; blue- aluminium. A diagonal indicates the beam's axis. The small (virtual) thimble detector set in the channel is shown in red

Fig. 4). This virtual thimble in the MCNP model was made of an absorbing material, and we used the MCNP's 'detector tally', which estimates the probability of every calculated neutron to scatter and arrive inside the base of the thimble. The thimble was close and wide enough to reach plausible statistics for accurate flux determination. Comparison shows that the flux estimation of the SALAMI-model is lower than the flux outcome of the thimble detector tally of MCNP by only 5%. The fact that the SALAMI estimate is low is consistent with the underlying assumption that the scattering is isotropic. In fact, especially in water, a scattered neutron tends not to change much its direction, and since the flux diminishes with the distance from the core, there are more neutrons going away from the core, and thus there are more neutrons scattered towards the camera than in an isotropic case.

Another route to validate the predictions was using past measurements. This was done with the available data, but subject to errors due to unknowns in the real camera structure, since the IRR1 neutron camera was built in the 1960's. The MCNP model predicted flux (both thermal and epithermal) fits the activation measurement in the water layer in front of the channel within the measurement error ($\pm 25\%$). This provides additional validation to the MCNP model, and specifically strengthens the confidence in the calculation results of the flux in the relevant layers.

The flux at the imaging plane has been measured using gold foil activation. Table 1 summarizes our predictions compared to the measurements done at the end of 2015, showing a factor of ~ 2 discrepancy. The predictions include the channel's transmission factor, which is estimated based on incomplete data. Note that the channel attenuation factor is about 10^{-7}, and includes the geometric factor ($(L/D)^2$) and attenuation by material in the beam's way, such as aluminium, air and especially the bismuth filter. The latter could be responsible for the discrepancy between the calculation of the flux and the measured value, since its cross section depends on temperature [Freund 1983] and on the crystal's structure [Adib 2003], and we do
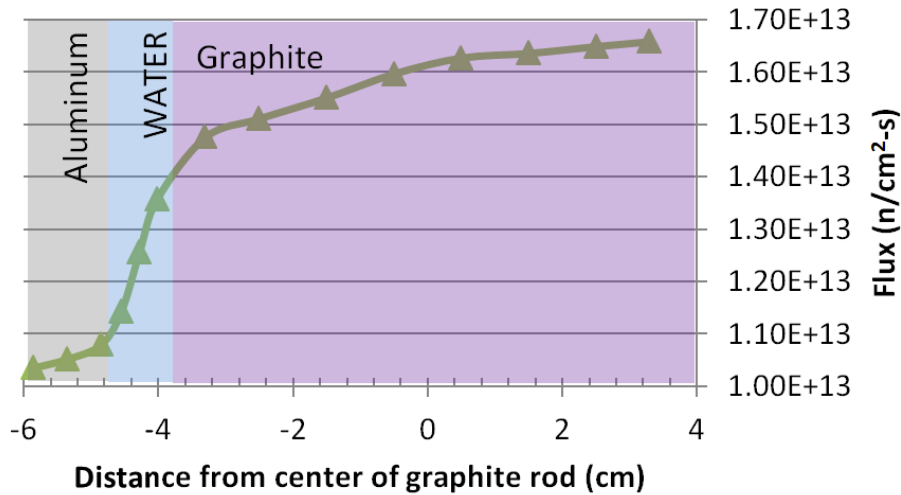
Figure 5: Thermal flux in layers in front of channel, according to MCNP calculation of IRR1. The colour shades indicate the layer material. Statistical errors of the points are of about 1%. The core is to the right, and the NC channel is to the left.

not have the information of its temperature in the time of measurement, nor on its crystalline condition after tens of years of radiation exposure. The degree of evacuation of the channel volume from air is not fully known either. The spatial flux variation span is a little higher than predicted, which may be attributed to the flux flattening device, introduced in this NC more than 40 years ago [Kedem 1972], and optimized for a specific and naturally different flux distribution.

Core configuration	measured thermal flux $10^6 \frac{\mathrm{n}}{\mathrm{cm}^2\mathrm{s}}$	Calculated flux $10^6 \frac{\mathrm{n}}{\mathrm{cm}^2\mathrm{s}}$
2015 #4 (5MW)	0.6-1.0 (mean=0.73)	1.5-2.0 (mean=1.7)
2015 #5 (3MW)	0.7-1.0 (mean=0.87)	1.3-1.6 (mean=1.4)
2017 (3MW)		1.5

Table 1: Comparison of measurements to layer-model calculations of the thermal flux at the imaging plane. The span represents the variation of the thermal flux at different locations on the image plane. Errors: measurements: $\pm 15\%$, calculations: $\pm 20\%$ (including unknowns in channel structure)

We also compared the measured cadmium ratio (CdR) to the SALAMI prediction. This value is determined by comparing gold foil neutron activation with and without a Cd shield. The activation of gold covered with Cd is mainly (90%) due to the absorption of epithermal neutrons at the gold resonance energy ($\sim 5 eV$), so higher CdR means the flux is more purely thermal. The calculated CdR at the water channel was within the measurement error ($CdR \approx 3 \pm 15\%$). For estimation of the CdR at the imaging plane we applied the SALAMI method in a similar fashion as described above, just with flux in the $5\,eV$ resonance energy vicinity, and the appropriate cross sections. Our prediction, based on the MCNP simulations of the cores, was used with the estimated (energy dependant) channel attenuation, and was nearly twice as high as the measured values. A possible reason for this discrepancy, that have some supporting indications from past measurements, is that the aperture material is not as effective in blocking epithermal flux as it is with thermal neutrons, thus the effective aperture diameter for the former is not known and the actual epithermal flux (proportional to D^2) may be very different than the calculated value.

The SALAMI-model makes it easy to calculate the sensitivity of the results to different core

parameters. We found that when the control rod nearest to the channel is raised by 10% of their full range the NC flux rises by 7% from the nominal case. This effect is explained by the fact that the NC channel is higher than the middle of the core, so when the control rod is raised the flux near the channel entrance is higher. The sensitivity of the total NC flux to the actual width of the water gap in front of the channel is about 2% per one mean-free-depth ($\delta \sim 2.5mm$) of increase in width. This low sensitivity is probably a result of the fact that this diffusive layer comes in addition to a much wider graphite layer ($W/\delta \sim 3.5$).

The ease of calculation provides an opportunity to optimize the core for high NC-flux-per-MW. Since the flux in the water layer is responsible for the majority of ballistic neutrons arriving at the film, we permutated the fuel rods' placements and, in light of Eq. (9), calculated the flux at the water's sampling depth. Preliminary search found configurations with a flux increase of about 50%, without substantial degradation of other core characteristics (such as criticality or control rod reactivity).

4   Conclusions

We presented the stacked layers Monte-Carlo incident neutron (SALAMI) calculation method, which estimates the neutron flux at the imaging plane of a neutron camera (NC) based on the calculated flux at several sites in material layers near the reactor core. This method is validated by full MCNP calculations of a smaller-scale NC, and by past measurements. This method is considerably faster than using a full Monte-Carlo calculation of the whole camera.

Overall, the calculations overestimate the flux at the NC image plane by a factor ~ 2 compared to the results of gold activation measurements in IRR1. We believe that this factor is related to uncertainties in the transparency of materials in the NC, mainly that of the Bismuth attenuator.

The understanding of the main contributing factors for the camera flux and the ease of calculation prove useful for core layout optimization. Preliminary results suggest a possible 50% increase of yield of the IRR1.

Further measurements are planned to validate the method and resolve some of the unknowns in the camera structure. The implementation of the optimized core will assert the applicability of this work.

The method is relevant not only for reactors but also for radiography with other neutron sources, such as accelerator bases neutron sources.

5   References

[Adib 2003] Adib, M., et al, Rad. Phys. Chem. **66** (2003)
[Duderstadt 1979] Duderstadt J. J. and Martin, W., *"Transport theory"* (1979), Wiley
[Freund 1983] Freund K., Nucl. Inst. Meth. **213** (1983) 495-501
[Kedem 1972] Kedem D. et al, Nucl. Inst. Meth. **102** (1972) 87-89
[Krakovich 2016] Krakovich, A. et al., Proceedings of the 28th Israeli Nuclear Society Conference, 12-14 April 2016, Tel-Aviv, Israel (2016)